Eur. Phys. J. B **14**, 239–244 (2000)

THE EUROPEAN PHYSICAL JOURNAL B

EDP Sciences

Experimental determination of the translational kinetic energy of liquid and solid hydrogen

M. Celli[1], D. Colognesi[2,3], and M. Zoppi[1,a]

[1] Consiglio Nazionale delle Ricerche, Istituto di Elettronica Quantistica, Via Panciatichi 56/30, 50127 Firenze, Italy
[2] Rutherford Appleton Laboratory, ISIS Neutron Facility, Chilton, Didcot, Oxon, OX11 0QX, UK
[3] Consiglio Nazionale delle Ricerche, Gruppo Nazionale di Struttura della Materia, Viale dell'Università 11, 00185 Roma, Italy

Received 9 June 1999

Abstract. TOSCA is a novel inelastic spectrometer operating on the pulsed neutron source ISIS (UK). It covers a wide momentum and energy range, even though its kinematic region is close to a line in the (k, E) plane. Its use is mainly intended for vibrational spectroscopy. However, taking advantage of its good resolving power, we have carried out a test experiment aimed to use this instrument to measure the centre of mass kinetic energy of molecular hydrogen. The experiment was successful and we have obtained the translational kinetic energy of liquid and solid para-hydrogen improving the overall accuracy by almost an order of magnitude with respect to previous determinations. The data are compared with the results of a Path Integral Monte-Carlo simulations with almost perfect agreement. We have demonstrated that TOSCA can be used for measuring the translational kinetic energy of small molecular systems, taking advantage of the intrinsic incoherence that is introduced in the scattering process by the intra-molecular transitions.

PACS. 61.12.Ex Neutron scattering techniques (including small-angle scattering) – 64.70.Dv Solid-liquid transitions – 67.90.+z Other topics in quantum fluids and solids; liquid and solid helium dynamics

1 Introduction

Deep inelastic neutron scattering (DINS) is generally used to determine the momentum distribution of simple monoatomic systems. In fact, when the momentum transferred from the neutron to the target nucleus becomes so large that the interference effects due to the correlation between neighbours becomes negligible, then the incoherent approximation holds and the process simply becomes a sum of single-atom scattering events. Thus, the intermediate scattering function becomes:

$$F(\mathbf{k},t) = \left(\frac{1}{N}\right) \sum_i \langle \exp\{-\mathrm{i}\mathbf{k}\cdot\hat{\mathbf{r}}_i(0)\} \exp\{\mathrm{i}\mathbf{k}\cdot\hat{\mathbf{r}}_i(t)\}\rangle \tag{1}$$

where $\hbar\mathbf{k}$ is the momentum transfer, and $\hat{\mathbf{r}}_i(t)$ represents the Heisenberg operator for the position of the target nucleus i at time t. As the magnitude of $|\mathbf{k}|$ increases, in the limit of $|\mathbf{k}| \to \infty$, the Impulse Approximation (IA) applies which reduces the intermediate scattering function to [1]:

$$F(\mathbf{k},t) \to F_{\mathrm{IA}}(\mathbf{k},t) = \exp\left\{\mathrm{i}\frac{E_{\mathrm{r}}}{\hbar}t\right\} \langle \exp\{\mathrm{i}\mathbf{k}\cdot\mathbf{v}t\}\rangle \tag{2}$$

where $E_{\mathrm{r}} = \hbar^2k^2/2m$ is the recoil energy and $\mathbf{v} \equiv \mathbf{v}(0)$ is the velocity of the target particle at time $t = 0$. Within the IA, the system is approximated by the ideal gas model and the dynamic structure factor becomes simply:

$$S(\mathbf{k},\hbar\omega) = \int \mathrm{d}\mathbf{p}\, n(\mathbf{p}) \delta(\hbar\omega - E_{\mathrm{r}} - \hbar\mathbf{k}\cdot\mathbf{p}/m) \tag{3}$$

where $\mathbf{p} = m\mathbf{v}$ is the momentum of the target particle and $n(\mathbf{p})$ is the momentum distribution [2,3].

Within the validity range of the IA, one has a direct experimental access to the momentum distribution of the particles. This is of a marginal interest for classical systems, where the distribution of the momentum variable is known to follow the classical Boltzmann statistics. However, it becomes of paramount importance in quantum systems where Bose-Einstein or Fermi-Dirac statistics are ruling the dynamic behaviour of the sample [4]. In particular, a direct access to the atomic momentum distribution allows the determination of the single particle density matrix by means of a simple Fourier transform.

A special case, where the application of the DINS technique is also useful, is the transition region between the classical and the quantum behaviour of simple dense systems [5–20]. This is the region where the de Broglie wavelength becomes sizeable but still does not exceed the size of the molecular diameter. In this case, the exchange

[a] e-mail: zoppi@ieq.fi.cnr.it

quantum statistics does not play an effective role and the particles are still distinguishable. Here, the Boltzmann statistics still applies, but the system cannot be considered classic any more as quantum diffraction effects play a relevant role. At any rate, the second moment of the momentum distribution gives a measure of the average kinetic energy of the particle and this quantity, in general, is not simply given by the classical expression $E_{\rm k} = \frac{3}{2}k_{\rm B}T$. A comprehensive review of the field can be found in reference [4]. More recent literature gives an account of the experimental work done on condensed noble gas systems [5–7] and in particular on liquid ^{4}He [8–16].

The results on liquid helium reported in reference [9] show a very interesting feature, which is peculiar of a quantum system. The experiment, carried out at constant temperature, results in a behaviour of the single particle kinetic energy that increases by increasing the density of the liquid. The density dependence of the kinetic energy in condensed systems is a direct consequence of the Heisenberg uncertainty principle. By decreasing the volume available to the atomic wave function, the fluctuation in the momentum space is increased and this results in an increase of the mean atomic kinetic energy. Thus, the density rise of the kinetic energy appears as a direct consequence of the reduction of the free volume that is available to each particle.

In a recent article [16] we have described the density behaviour of liquid and solid ^{4}He on the isotherm $T = 6.1$ K. In Figure 2 of reference [16] we reported the experimental results for the kinetic energy of helium as a function of the density. From the figure, it appears that the solid phase data do not agree with the extrapolation that can be inferred from the fluid phase data and that they are characterized by a smaller value of the kinetic energy. In fact, at fixed density, the kinetic energy in the solid phase is lower than the corresponding value extrapolated from the isotropic phase. Thus, we have shown that the density behaviour of the kinetic energy is driven not only by the free volume effect but, crossing the freezing transition, is also influenced by the development of properties that are somehow characteristic of the crystal structure.

It would be interesting to check whether this behaviour is peculiar of helium or is a common feature of quantum liquids. However, since the quantum properties of neon are much smaller than those of helium, neon cannot be considered for testing this hypothesis and the only left alternative is with hydrogen. Unfortunately, previous experimental investigations aimed at measuring the translational kinetic energy of hydrogen have provided data with rather large error bars [18,19]. Therefore, it would be virtually impossible to test this effect using the same instrument, or another one with a similar resolution.

2 The advantages of TOSCA

TOSCA is a crystal analyser inverse geometry spectrometer [21]. The incident neutron beam extends on a rather large energy range and the energy selection is carried out, on the secondary neutron path, using the (002) Bragg reflection of graphite single crystals at a nominal angle of 45°. This fixes the neutron energy to $E_1 \cong 3.6$ meV. Higher order Bragg reflections are filtered out by a thick (15 cm) beryllium block cooled down to $\sim$ 50 K. This geometry allows to cover an extended energy range, even though the fixed position of the crystal analysers implies a variation in $|\mathbf{k}|$ that is a monotonic function of E. The resolving power of TOSCA is rather good ($\Delta E/E \sim 2.5\%$) and is due to improve in the next future. Moreover, the extended spectral range makes this instrument a neutron equivalent of a Raman spectrometer. Thus, intramolecular transitions can be easily observed with TOSCA, well beyond the first vibrational transition of molecular hydrogen (we remind that this is placed at 514.5 meV or 4 150 cm^{-1}). However, due to the recoil energy, the observed shifts are much greater on a neutron spectrometer.

The Raman spectrum of liquid hydrogen is characterized by the intra-molecular transitions (rotations and vibrations). However, on the Stokes (energy-loss) side of each intra-molecular line, a side phonon band of intermolecular origin is visible [22], which originates from the same mechanism that produces the broad, quasi-elastic, band that is attributed to collective, multi-phonon, excitations. Similar concepts can be applied to the neutron scattering spectrum of molecular hydrogen. Here, the fundamental difference between the quasi-elastic (no intramolecular transition is involved) and the inelastic contribution (one or more intra-molecular transitions are involved) is due to the different weight of the self and distinct translational components. In fact, in the quasi-elastic spectrum, the Van Hove [23] formulation applies and the contribution to $S(\mathbf{k}, \omega)$ is a mixing of the two components, as in any monatomic liquid. However, only the self term contributes to the inelastic neutron spectrum [24].

In some sense, TOSCA can be considered the neutron equivalent of an optical Raman spectrometer. However, in this case, the momentum transfer changes with the energy shift. In the low-energy region of the spectrum, the size of the momentum transfer remains within limits that are similar to the reciprocal of the intermolecular distances between neighbours. In this case, the self contribution to the scattering function is known to carry information on the velocity-velocity correlation function and the self-diffusion coefficient [25]. In the high-energy region, the momentum transfer grows to such an extent that the scattering function is expected to merge into the IA. Therefore, the spectrum carries information relative to the momentum distribution of the centres of mass. Even though the transition between the two regimes is not clearly defined, one would guess that it lies beyond the first peak of the intermolecular $S(k)$ (~ 2 A^{-1}) in the region where $S(k)$ becomes ~ 1 (*i.e.* $k \sim 6{-}8$ A^{-1}). The k-region spanned by TOSCA goes well beyond this interval.

If pure liquid para-hydrogen is considered, the inelastic neutron spectrum becomes extremely simple. Since the transitions to the even states ($J = 0 \rightarrow J' = 2,\ 4,\ \ldots$) are weighted by the small hydrogen coherent cross section, their intensity is two orders of magnitude smaller than the transitions to the odd states. Thus, the observed spectrum

reduces, for any practical purpose, to the odd rotational transitions ($J = 0 \rightarrow J' = 1,\ 3,\ \ldots$). In addition, due to the small moment of inertia of hydrogen, the rotational transitions are well separated ($J = 0 \rightarrow J' = 1$ implies an energy jump of 14.7 meV, while $J = 0 \rightarrow J' = 3$ corresponds to a jump of 88.2 meV). As a consequence, the superposition of the different bands is small and each band can be analysed separately.

If we focus our attention on the first rotational transition ($J = 0 \rightarrow J' = 1$), the double differential cross section is given by:

$$\frac{\mathrm{d}^2\sigma}{\mathrm{d}\Omega \mathrm{d}\omega} = \frac{k_1}{k_0}\frac{\sigma_\mathrm{i}}{4\pi}\Sigma(k,\omega) = \frac{k_1}{k_0}\frac{\sigma_\mathrm{i}}{4\pi}\left|f(k)\right|^2_{0\rightarrow 1} S_\mathrm{self}(k,\omega) \otimes \delta(\omega - \omega_{0\rightarrow 1}) \quad (4)$$

where σ_i is the hydrogen incoherent cross-section, $f(k)$ is the intra-molecular form factor and $S_\mathrm{self}(k,\omega)$ is the self, molecular, dynamic structure factor. The symbol $\otimes$ represents a convolution and δ is the Dirac delta-function. The cross section can be evaluated along the kinematic path of TOSCA to derive a theoretical distribution, provided a suitable model is given for $S_\mathrm{self}(k,\omega)$.

3 The experiment

The measurement was carried out at seven thermodynamic points. Five were selected in the liquid phase and two in the solid. After performing the background measurements of the empty cryostat, we cooled the empty container at the desired temperature ($T = 17.2$ K) and we measured its time-of-flight (TOF) spectrum. Then, hydrogen was allowed to condense in the scattering cell. This was made of aluminium, 1 mm thick walls, and with cylindrical-slab geometry. The sample thickness was 1.5 mm and the cell diameter (50 mm) was a little larger that the beam cross-section. The pressure of the gas handling system was set to $p = 0.43$ bar in order to make sure that the cell was filled with liquid (the vapour pressure at $T = 17.2$ K is 0.36 bar).

At the bottom of the scattering container, out of the neutron beam, we had inserted some powder of paramagnetic catalyst made of Cr_2O_3 and γ–Al_2O_3 in order to accelerate the transition rate from ortho- to para-hydrogen. The relative concentration of the two species was monitored looking at the scattering spectrum. In particular, we could observe the progressive disappearance of the $J = 1 \rightarrow J' = 1$ transition, that is weighted by the incoherent cross section of the proton, from the quasi-elastic portion of the spectrum. When this spectral component was below the limit of detectability (in practice, masked by the $J = 0 \rightarrow J' = 0$ transition, that is weighted by the coherent cross section of the proton) we assumed that the equilibrium was reached. The equilibration process takes, in our case, about 20 hours. The estimated concentration of para-hydrogen, based on the theoretical analysis, is assumed to be 99.96%. Then, we started recording the scattering spectrum up to an integrated proton current of 2 271 μAh. The following spectra were taken in a similar way, after changing the temperature and pressure of the sample, performing some short test spectra, to ensure that the sample was thermodynamically stable.

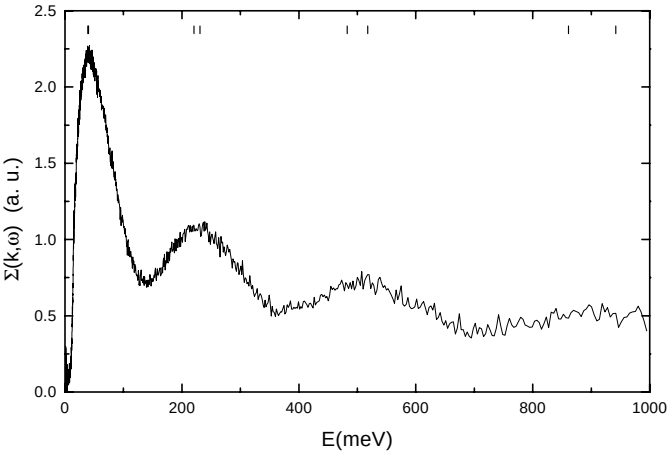

Fig. 1. Experimental raw inelastic spectrum measured on liquid para-hydrogen at $T = 17.2$ K and $p = 0.43$ bar. Each peak represents a rotational transition starting from the ground level $J = 0$. The transition to the even levels are weighted by the small coherent cross-section, therefore only the transitions to the odd levels $J' = 1,\ 3,\ 5,\ 7$ are visible. The small vertical bars on the top of the graph represent the resolving power of the spectrometer.

The stability of the thermodynamic conditions during the experiment was very good. The temperature fluctuations never exceeded 0.1 K and the pressure stability was strictly related to this value, thanks to the very good realisation of the gas handling system. The densities of our samples were derived according to reference [26]. The full set of parameters characterizing the present experiment is reported in Table 1.

4 Data analysis

The design of TOSCA is such to allow time-focusing on the detector plane. However, the spread in the scattering angles (ranging between $\sim 129°$ and $\sim 140°$) would imply some deterioration of the instrument resolving power. Therefore, we have analysed separately each detector spectrum. The final spectra, converted to energy shifts, where eventually added together to improve the statistical accuracy.

Figure 1 shows the raw spectrum of liquid para-hydrogen at $T = 17.2$ K and $p = 0.43$ bar. The rotational transitions are shifted by the Doppler effect due to the molecular recoil. Four rotational transitions are clearly visible in the spectrum which correspond to the intra- molecular transitions $J = 0 \rightarrow J' = 1,\ 3,\ 5,\ 7$, respectively. Despite the small thickness of the sample, some multiple scattering was expected. A rough simulation of this contribution suggests a smooth spectral shape, slowly increasing with the energy transfer. Accordingly, we

Table 1. Thermodynamic conditions of the measured hydrogen samples, including the theoretically calculated para-hydrogen percentage, [p−H_2], and neutron integrated current, I.C. The last two columns report the fitted centre of mass mean kinetic energy, E_k^{exp} and the PIMC simulation results, E_k^{pimc}. For the PIMC results we assume a uniform uncertainty of 0.6 K. The first two lines refer to the solid phase, the others are relative to the liquid phase. The triple point temperature is $T_{TP} = 13.803$ K.

T (K)	n (nm^{-3})	p (bar)	[p−H_2] (%)	I.C. (μAh)	E_k^{exp} (K)	E_k^{pimc} (K)
12.2(2)	26.02(2)	0.05(1)	100.00	1490	68 ± 2	70.0
13.2(2)	25.91(2)	0.09(1)	100.00	1792	69 ± 1	70.3
14.3(2)	22.91(6)	0.16(1)	99.99	2368	61 ± 1	57.4
15.7(2)	22.52(6)	0.24(1)	99.98	1917	60.0 ± 0.6	60.7
17.2(2)	22.10(6)	0.43(1)	99.96	2271	60.6 ± 0.6	61.2
19.2(2)	21.50(6)	0.82(1)	99.88	2310	62 ± 1	61.4
21.2(2)	20.83(9)	1.34(1)	99.71	1344	62 ± 2	61.9

analysed the data allowing for a polynomial background of that shape.

The intermolecular structure factor of liquid para-hydrogen has not been measured yet. However, we can infer its main features from the corresponding quantity for liquid deuterium [27]. In this case, $S(k)$ becomes virtually ~ 1 for values of $k \geq 6$ A^{-1}. The boundary between the first and second transition lies at ~ 130 meV, which corresponds to a momentum transfer $k \sim 9$ A^{-1}. We expect that the $J = 0 \rightarrow J' = 3$ transition is already fulfilling the IA for the molecular centres of mass [18] or, at most, final states effects (FSE) can be included as small corrections [2]. Therefore, the spectrum beyond the first minimum can be fitted using the IA, *i.e.* using equation (3). In addition, we approximate the momentum distribution of the translational motion by a Gaussian shape. This is considered to be a good approximation for quantum Boltzmann liquids. In fact, while for normal liquid helium close to the λ-transition, or in the superfluid phase, the Gaussian approximation is known to fail [10,13–15], no such information is available at higher temperatures. The Gaussian approximation is found to be in good agreement with the experimental data in the case of liquid neon [13,28].

For each raw-data spectrum, we have fitted the region beyond the first minimum of the scattering function using the IA and a Gaussian shape for the momentum distribution. The energy position of the intra-molecular transitions, as well as their relative intensities, were kept fixed and we only allowed for the variation of a single overall intensity factor and the width of the Gaussian shape (two parameters). From the knowledge of the scattering angle, and by means of the energy and momentum conservation laws, it is possible to derive the dispersion relation $E(k)$, where E and k are the energy and the momentum transfer at the peak positions. If the IA holds, the peak of the n-th rotational excitation, $E_r^{(n)}$, in the scattering function, is placed at the recoil energy plus the excitation energy, $E_{0\rightarrow n}$ of the intra-molecular transition $J = 0 \rightarrow J' = n$:

$$E_r^{(n)} = \hbar^2 k^2 / 2m + E_{0\rightarrow n}. \quad (5)$$

Thus, leaving the recoil mass as a free parameter, a linear fit to the data should give the effective mass of the

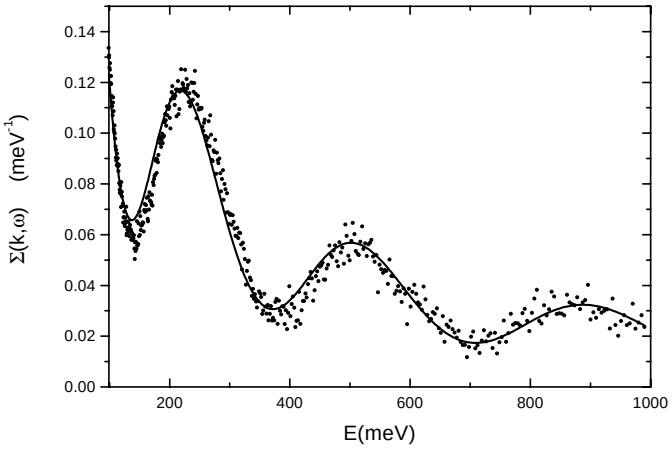

Fig. 2. Experimental inelastic spectrum measured on liquid para-hydrogen at $T = 14.3$ K and $p = 0.16$ bar after multiple scattering corrections. We do not consider the $J = 0 \rightarrow J' = 1$ transition because in this case the Impulse Approximation does not apply. The line represents the best fit to the data using the Impulse Approximation and a Gaussian function for the momentum distribution. From the fit we could extract the centre of mass kinetic energy, E_k^{exp}.

scattering centre. In fact, in the k-region explored by the present experiment ($k > 9$ A^{-1}), the observed spectrum appears very similar to the recoil spectrum of a monatomic sample with the various peaks shifted because of the different intra-molecular transitions. The fitted mass turns out $m = (1.99 \pm 0.01)$ amu., *i.e.* almost identical to the molecular mass of hydrogen (2.016 amu). Similar values for m, within the same statistical uncertainty (0.5%), were obtained for the other thermodynamic states.

To close up, the Gaussian approximation for the momentum distribution, together with the IA for the dynamic structure factor, represent a very good approximation to the spectral shape beyond the first peak of the spectrum. The result of the fitting is represented by the continuous line in Figure 3.

In any case, from the width of the momentum distribution (the second moment) we could estimate the kinetic energy of the molecular centre of mass. The important result of the present experiment is that the error bar

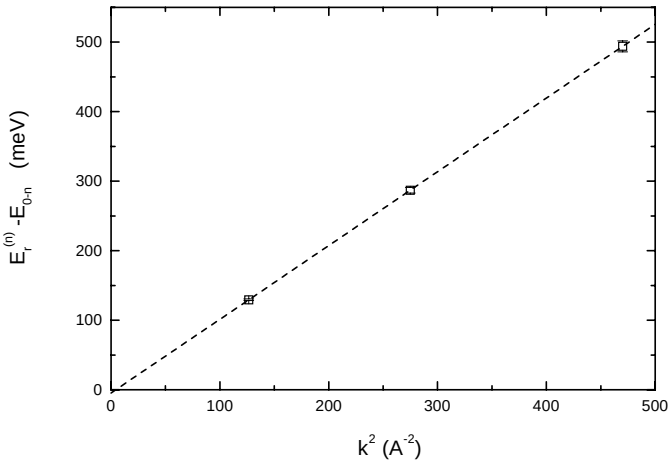

Fig. 3. Recoil energies, $E_{\rm r}^{(n)} - E_{0\to n}$, as a function of the square of the momentum transfer from the spectrum of liquid para-hydrogen at $T = 14.3$ K and $p = 0.16$ bar. The slope of the linear fit (dashed line) is proportional to the inverse of the recoil mass (see Eq. (5)) which turns out $m = 1.99 \pm 0.01$ amu. This demonstrates that we measure, indeed, the centre-of-mass kinetic energy.

attributed to this determination is improved almost by an order of magnitude with respect to previous experimental determinations going from an uncertainty of $\sim (6 \div 9)$ K to the present uncertainty of ~ 1 K.

5 Simulation

The computer simulations of liquid and solid para-hydrogen were carried out using the same technique, namely path integral Monte-Carlo (PIMC), that was used in reference [29]. The intermolecular potential was assumed to be pair-wise additive and the crystal lattice was assumed to be hcp. Several specific pair potentials are available in the literature and some recent experimental results using light scattering suggest that the Schaefer and Köhler potential [30] best represents the experimental results [31]. However, we used the semi-empirical model proposed by Norman *et al.* [32] because it is given in analytic form and the two isotropic components are very similar in the two potentials. In fact, since the molecular wave function for para-hydrogen in the ground level ($\nu = 0$, $J = 0$) is spherically symmetric, and this feature seems to be conserved even in the condensed phases (at least at not too high pressure), only the spherical component of the potential was used in the simulation.

The number of classical particles was set to $N = 108$. Although relatively small, this number should be sufficient to describe single particle properties such as the kinetic energy, which is our main concern here. The particles were assumed to obey Boltzmann statistics. All interactions were truncated spherically at a cut-off equal to half the minimum edge length of the box, and potential energies and pressures were corrected by integrating over a uniform density beyond the cut-off. The thermodynamic conditions were selected according to the temperature and density of the experimental points (see Tab. 1).

In all cases but one, the number of beads on the ring polymers (P, *i.e.* the Trotter number) was set $P = 32$. In one case, this number was varied in order to test the convergence of the simulations as a function of P. We used $P = 1$, 4, 8, 16 and 32. The rate of convergence of the results from the classical to the quantum mechanical behaviour was analysed by plotting $E_{\rm k}$ as a function of $1/P$. It turns out that $P = 16$ and $P = 32$ gave very similar results. Therefore, we assume the $P = 32$ value as the quantum limit and, from the difference between the $P = 16$ and $P = 32$ values, we estimate an error of 0.6 K for the simulation results.

Each simulation was started from a perfect hcp lattice and consisted of $10\,000 \times NM$ passes (*i.e.* moves per particle), after a $5\,000 \times NM$ passes equilibration stage. NM is the dilution factor; *i.e.* the number of passes performed before analysing the next configuration. We used $NM = 5$. Thus, averages were accumulated using 10 000 configurations out of each run that, in total, was obtained accumulating $N \times NM \times 10\,000$ Monte-Carlo moves (plus equilibration). The results of our simulation are reported in the last column of Table 1.

6 Discussion and conclusions

The results for the translational kinetic energy of liquid and solid para-hydrogen, that are reported in Table 1, are in very good agreement with the PIMC simulation. The two sets of data superimpose to each other within their respective error bars (we assume a generalised uncertainty of 0.6 K for the PIMC results).

Only in one case ($T = 14.3$ K, $n = 22.91$ nm^{-3}) there is an evident discrepancy between the experiment and the simulation results. For this point the simulation was repeated and extended. Without changing the results, however. The reason for the discrepancy came out clearly by comparing the radial distribution functions of the various simulations. In fact, it turns out that the radial distribution function for the two solid state simulations are almost exactly superimposed. The same happens for the $g(r)$ in the liquid state. However, the radial distribution function for the point at $T = 14.3$ K, $n = 22.91$ nm^{-3}, gives intermediate values between the two. This means that, in the simulation, this particular thermodynamic point, because of the model potential that is only an imperfect representation of the true one, happens to be in a meta-stable situation between the liquid and the solid state. Due to the smallness of the simulation sample, it is likely that a clear phase separation could not be achieved in the relatively short time of the simulation. At any rate, we cannot rely on this simulation point for our comparisons.

In conclusion, we have shown that TOSCA can be effectively used to measure the translational kinetic energy of molecular hydrogen in the condensed phases. The error bars associated with the present experimental determination are almost an order of magnitude better that the previous ones. The experimental results have been

compared with the PIMC simulation data of para-hydrogen in the same thermodynamic conditions. The agreement is very good and the two sets of data superimpose to each other, within their respective estimated errors.

We are confident that future planned experiments on the same system, taken at constant temperature, will help to shed some light on the general problem of the behaviour of the kinetic energy of quantum liquids across the freezing transition.

The superb technical assistance of the ISIS Instrument Division of RAL is gratefully acknowledged.

References

1. V.F. Sears, Phys. Rev. **185**, 200 (1969).
2. V.F. Sears, Phys. Rev. B **30**, 44 (1984).
3. S.W. Lovesey, *Theory of Neutron Scattering from Condensed Matter* (Clarendon, Oxford, 1987).
4. R.N. Silver, P.E. Sokol, *Momentum Distribution* (Plenum, New York, 1989).
5. D.A. Peek, R.O. Simmons, J. Chem. Phys. **94**, 3169 (1991).
6. D.A. Peek, M.C. Schmidt, I. Fujita, R.O. Simmons, Phys. Rev. B **45**, 9671 (1992).
7. D.A. Peek, I. Fujita, M.C. Schmidt, R.O. Simmons, Phys. Rev. B **45**, 9680 (1992).
8. V.F. Sears, E.C. Svensson, P. Martel, A.D.B. Woods, Phys. Rev. Lett. **49**, 279 (1982).
9. K.W. Herwig, P.E. Sokol, T.R. Sosnick, W.M. Snow, R.C. Blasdell, Phys. Rev. B **41**, 103 (1990).
10. T.R. Sosnick, W.M. Snow, P.E. Sokol, Phys. Rev. B **41**, 11185 (1990).
11. T.R. Sosnick, W.M. Snow, R.N. Silver, P.E. Sokol, Phys. Rev. B **43**, 216 (1991).
12. C. Andreani, A. Filabozzi, M. Nardone, F.P. Ricci, J. Mayers, Phys. Rev. B **50**, 12744 (1994).
13. R.T. Azuah, W.G. Stirling, H.R. Glyde, P.E. Sokol, S.M. Bennington, Phys. Rev. B **51**, 605 (1995).
14. R.T. Azuah, W.G. Stirling, H.R. Glyde, M. Boninsegni, P.E. Sokol, S.M. Bennington, Phys. Rev. B **56**, 14620 (1997).
15. K.H. Andersen, W.G. Stirling, H.R. Glyde, Phys. Rev. B **56**, 8978 (1997).
16. M. Celli, M. Zoppi, J. Mayers, Phys. Rev. B **58**, 242 (1998).
17. K.W. Herwig, M.C. Schmidt, J.L. Gavilano, R.O. Simmons, Jpn J. Appl. Phys. **26**, 445 (1987).
18. W. Langel, D.L. Price, R.O. Simmons, P.E. Sokol, Phys. Rev. B 38, 11275 (1988).
19. K.W. Herwig, J.L. Gavilano, M.C. Schmidt, R.O. Simmons, Phys. Rev. B **41**, 96 (1990).
20. C. Andreani, D. Colognesi, A. Filabozzi, M. Nardone, R.T. Azuah, Europhys. Lett. **37**, 329 (1997).
21. S.F. Parker, C.J. Carlile, T. Pike, J. Tomkinson, R.J. Newport, C. Andreani, F.P. Ricci, F. Sacchetti, M. Zoppi, Physica B **241-243**, 154 (1998).
22. M. Zoppi, L. Ulivi, M. Santoro, M. Moraldi, F. Barocchi, Phys. Rev. A **53**, R1935 (1996).
23. L. Van Hove, Phys. Rev. **95**, 249 (1954).
24. V. Sears, Can. J. Phys. **44**, 1279 (1966).
25. U. Balucani, M. Zoppi, *Dynamics of the liquid state* (Oxford University Press, Oxford, 1994).
26. R.D. McCarty, J. Hord, H.M. Roder, *Selected Properties of Hydrogen* (National Bureau of Standards, Washington, 1981).
27. M. Zoppi, U, Bafile, E. Guarini, F. Barocchi, R. Magli, M. Neumann, Phys. Rev. Lett. **75**, 1779 (1995).
28. D.N. Timms, A.C. Evans, M. Boninsegni, D.M. Ceperley, J. Mayers, R.O. Simmons, J. Phys. Cond. Matter **8**, 6665 (1996).
29. M. Zoppi, M. Neumann, Phys. Rev. B **43**, 10242 (1991).
30. J. Schaefer, W.E. Köhler, Z. Phys. D **13**, 217 (1989).
31. M. Moraldi, M. Santoro, L. Ulivi, M. Zoppi, Phys. Rev. B **58**, 234 (1998).
32. M.J. Norman, R.O. Watts, U. Buck, J. Chem. Phys. **81**, 3500 (1984).